ADVANCED MATERIALS TECHNOLOGIES
www.advmattechnol.de

Computationally Guided DIW Technology to Enable Robust Printing of Inks with Evolving Rheological Properties

*Maria Luisa Lopez-Donaire, Gonzalo de Aranda-Izuzquiza, Sara Garzon-Hernandez, Javier Crespo-Miguel, Miguel Fernandez-de la Torre, Diego Velasco, and Daniel Garcia-Gonzalez**

Soft multifunctional materials allow for mechanical sensing or actuation as a response to multiple physical stimuli, while providing material stiffness that mimic soft biological tissues (≈1–10 kPa). One of the main bottlenecks in the state of the art relates to the difficulty for manufacturing complex shapes when using inks whose properties significantly change over the printing time. To overcome this issue, the implementation of a hybrid (theoretical-experimental) framework that allows optimal printability of time-dependent viscosity inks by using the direct ink writing technology. Although the rheological properties of the ink vary during printing time, a combination of theoretical and experimental methods provides evolving printing conditions that ensure efficient and robust printability over the process. The method removes the need of introducing additives to the ink. To enable this technology, an in-house printer that provides flexibility to modulate the extrusion pressure over printing time is developed. The method is validated by manufacturing magnetorheological elastomers and conductive soft materials for specific bioengineering and soft electronics applications.

1. Introduction

The advance in material science and structural engineering has led to materials that not only provide structural support but also other functionalities, that is, multifunctional materials.[1] Recent works on multifunctional materials have opened new routes in different application fields, especially in the soft-robotics,[2,3] bioengineering,[4–6] and sensor-actuator ones.[7–9] These consist of soft materials filled with particles sensitive to external stimuli, such as external magnetic or electric actuation.[10–13] Thus, their mechanical behavior can be modulated remotely, resulting in structural and functional components for a wide range of vanguard applications like soft robotics, and novel components of biomedical instrumentation including soft tools for surgery, diagnosis, and drug delivery.[14] Additionally, these functionalities act as the ideal framework to recreate and model relevant biophysical conditions and events by creating complex physical patterns.[15–17] To date, most multifunctional materials are manufactured mainly using molding techniques. This fact greatly limits the customization and efficiency of the process. Other issue when working with traditional manufacturing methods and very soft materials arises during demolding, when certain regions of the components can be significantly damaged, especially when these present complex geometries. Another important limitation relates to the design and production of multicomponent structures composed of heterogeneous material regions, that is, functionally-graded materials.[17] To overcome such limitations, additive manufacturing (AM) technologies, also referred to as 3D printing technologies, have become the preferred option for the fabrication of these structures.[18–21] To increase the performance and marketability of these applications, 3D printing is presented as an ideal candidate to refine morphological and functional characteristics of soft material constructs, enabling the creation of anisotropic conditions along complex geometries.[22,23] The most common manufacturing techniques of soft responsive polymers based on AM are direct ink writing (DIW),[18,24–29] ink-jet printing (DOD),[30–33] light-assisted AM,[19,34] and selective laser sintering (SLS).[35,36] Photopolymerization based technologies (SL) have the best resolution. However, the problem with SL is the need of a photocurable silicon. In addition, if traditional elastomers, for example, polydimethylsiloxane (PDMS), are used with this technology, they need to be modified physicochemically to present a photocurable nature, compromising their final performance.[37,38] Moreover, although DIW resolution is limited by the nozzle diameter, it offers great opportunities to 3D print

M. L. Lopez-Donaire, S. Garzon-Hernandez, J. Crespo-Miguel, M. Fernandez-de la Torre, D. Garcia-Gonzalez
Department of Continuum Mechanics and Structural Analysis
Universidad Carlos III de Madrid
Avda. de la Universidad 30, Leganés, Madrid 28911, Spain
E-mail: danigarc@ing.uc3m.es
G. de Aranda-Izuzquiza, D. Velasco
Department of Bioengineering and Aerospace Engineering
Universidad Carlos III de Madrid
Avda. de la Universidad 30, Leganés, Madrid 28911, Spain
The ORCID identification number(s) for the author(s) of this article can be found under https://doi.org/10.1002/admt.202201707.

DOI: 10.1002/admt.202201707

materials with mechanical properties close to the bulk material. In addition, this technology does not require the application of UV light, which may be a limitation in the presence of opaque fillers (essential for multifunctional materials). An important gap in the current state of the art relates to the impossibility of using time-varying polymeric (mainly elastomeric) matrices in a robust and efficient manner.[39,40] Current solutions to obtain complex, for example, PDMS-structures consist in building 3D sacrificial molds,[41] in using a support bath via free-form reversible embedding,[42] or in blending two silicone elastomers, that is, a shear-thinning PDMS and a low-viscosity PDMS.[40] Many of these materials, however, have been demonstrated to be ideal candidates for several applications like soft-electronics, soft-robotics, or even as artificial active tissues.[9,17,43,44] The main issue when printing these materials is that, at the time of mixing, these behave as a pure liquid hindering the printing.[40] In addition, the rheological properties of such material continuously evolve drastically changing the optimal printing conditions over time.[20,45] These changes in material properties are even more abrupt in the presence of solid fillers (the active phase of the multifunctional material).[46–48] To overcome these issues, previous works used inks that either introduce additives to enhance the printability of the material or combined different elastomeric matrices.[18,24,49,50] The addition of other phases or additives not only impacts the material printability, but also its final properties. Hence, alternatives keeping the matrix and filler phases intact would be helpful to enable the printing adaptation of multifunctional materials used by molding techniques straightforwardly. However, such alternatives may need to consider the evolution of the viscosity with time as it has a great influence on the pressure needed during the printing process to provide flow control (especially for longer periods of printing time or multiple scaffolds).

Therefore, the following main impediments exist for using soft biological tissue-like elastomers in DIW multifunctional materials. 1) Lack of a consistent methodology to evaluate the time-window that allows for printing time-varying (ongoing curing) inks. 2) Lack of methodology to determine optimal printing conditions (i.e., flow rate, printing speed, pressure, and temperature profiles, etc.) over the time-window that enables the printing of the ink. 3) Lack of a robust implementation method to translate the previous information to a functional 3D printer. Overall, there is a lack of printing technologies that allow for the accurate material deposition and posterior shape fidelity of the printed construct when using time-varying inks. To overcome the limitations stated before, this work aims at providing a methodology to answer the two main questions depending on the ink used: i) the optimal time window of the curing process that allows for robust printability of the material; and ii) the printing conditions that provide a consistent filament formation over the printing process. To this end, the experimental characterization of the curing behavior of time-dependent systems is determined by combining tests with a rheometer and with a universal testing machine. The ink-viscosity evolution with time is first determined by oscillation and rotational experiments using rheology. On the other hand, a testing device equivalent to the pneumatic extruder used in the printer is designed to be coupled to the universal testing machine using the compression plate mode. This platform allows to obtain the time evolution of the pressure profile for a given ink and specific manufacturing conditions. Such a pressure profile is then used as an input for our new in-house 4D printer to ensure a constant flow rate during the printing process. The experimental data obtained from rheology are processed and incorporated in a theoretical model that guides the design of the final printing process. This model feeds the computer-controlled robotic dispenser ensuring that the extrusion printing speed is constant during all the manufacturing process. An overall workflow of the hybrid printing framework developed herein is presented in **Figure 1**. This methodology is finally validated with three applications: i) the manufacturing of magnetorheological elastomers (MREs) comparing their magneto-mechanical behavior against molded samples; ii) the development of multicompartment MREs for mechanobiology testing; and iii) the production of soft conductive materials for soft electronic sensors.

2. Results

2.1. Rheological Characterization to Determine the Print-Window of Multifunctional Materials and Experimental Procedure to Obtain Constant Reactive Ink Flow Over Time

The DIW of multifunctional materials whose rheological properties vary with time at printing-condition temperatures is an open question in the scientific community. This manufacturing technology is fed by a material precursor (i.e., ink) in liquid-phase that is pushed through a needle in the form of a filament. The formation of a consistent filament depends on different operational variables such as the nozzle diameter and geometry, or the extrusion speed; and on the rheological properties of the ink, that is, viscosity or shear moduli. Whereas the operational variables can be easily set, the control of those related to the ink can be especially challenging when using thermocurable or reactive inks.[51,52] In this regard, MREs composed of, for example, soft PDMS-based matrices filled with magnetic particles, are very convenient for applications where soft biological tissue-like multifunctional materials are needed.[9,17,53] These materials are initially in a fluid-phase state that evolves with time during curing to a solid state. This curing process is accelerated with the presence of magnetic particles and governs the evolution of the ink properties such as viscosity or shear moduli. Note that these material changes are not linear but present drastic changes over curing.

Prior to the development of the experimental methodology to identify optimal DIW conditions depending on the material printed, we developed an in-house printer that allows to translate these findings to real implementation (see Figure 1 and Experimental Section). The printer presents an open software that can be used to define a pressure profile over time on the cartridge that contains the MRE precursor. Therefore, this printing variable can be modulated during the manufacturing process to compensate changes in the rheological properties of the ink (see Experimental Section for more details on the printer characteristics). Note that this technology was chosen instead of mechanical screwing to minimize material dripping without retractions and provide the pressure flow

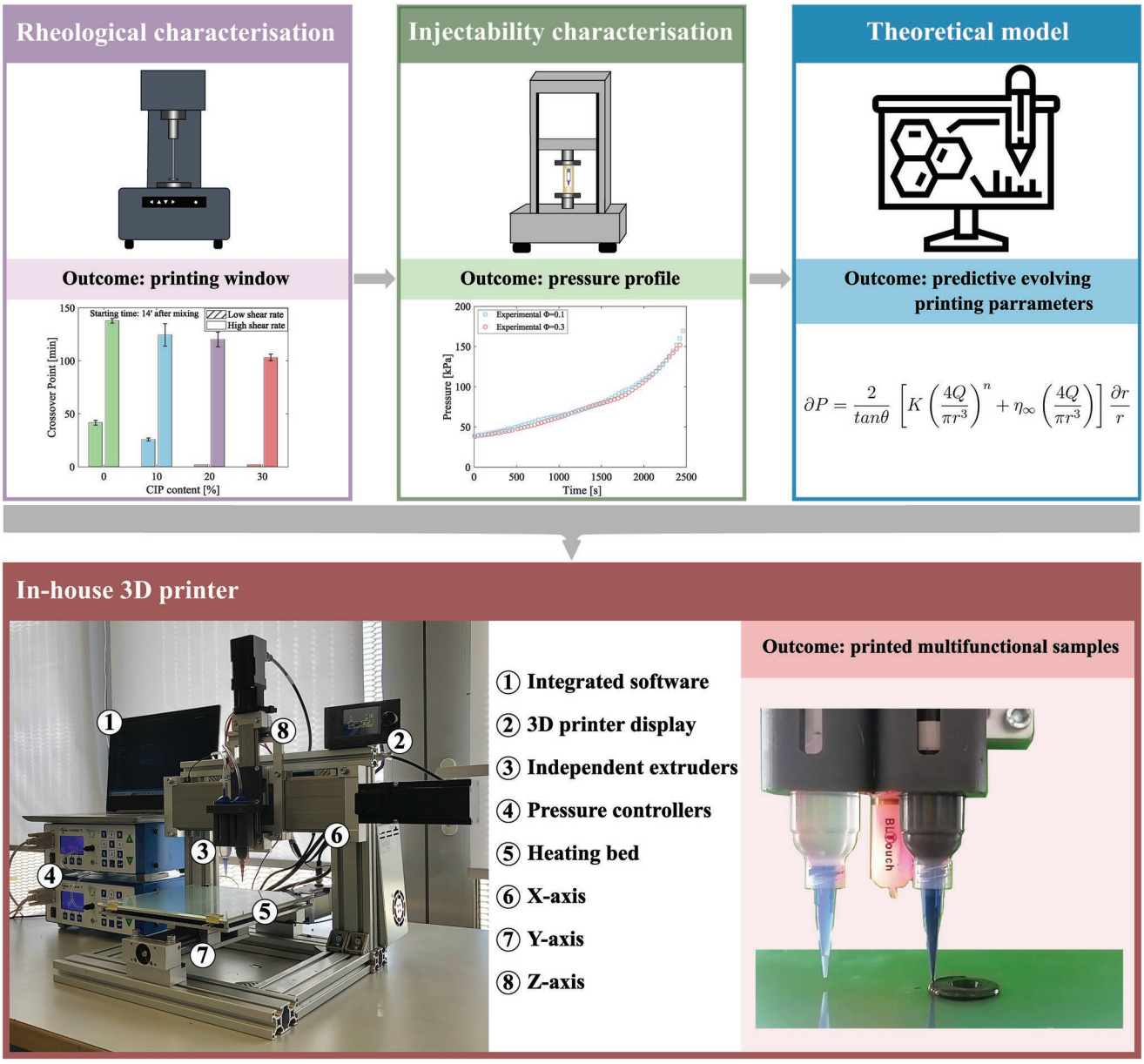

Figure 1. Complete workflow of the proposed experimental-theoretical framework for direct ink writing (DIW) of reactive inks. Overall workflow of the hybrid DIW framework to print multifunctional materials based on thermo-curable or reactive inks. The method first characterizes the rheological properties of the pre-cured ink over time at different shear rates. This information provides the printing time-window for the specific ink. An injectability characterization test is performed within the obtained print-window to define the pressure profile needed to ensure constant flow rate over time. The previous experimental data feeds a theoretical model that combines the rheological behavior of the ink with geometrical properties of the printing system, to finally predict the evolving printing parameters over time. These printing parameters feed our in-house 3D printer allowing for multimaterial printing of soft functional materials.

instantaneously. This feature is essential as the printing of multimaterial samples requires the instantaneous activation and interruption of the ink flow providing a robust spatial dispensation of complex patterns, which will determine the multifunctional response of the material. Such an instantaneous control of the flow rate cannot be ensured with positive displacement extrusion systems, especially when using non-Newtonian inks. Hence, the determination of such an extrusion-pressure is essential for a regular printability over time. In addition to material changes due to curing, during the printing process, the ink presents different mechanical states: i) a resting state in the cartridge; ii) high shear rate conditions when passing through the nozzle; and iii) a new resting state once deposited on the platform. These different shear rates also have an important impact on the ink behavior due to its effective viscosity, especially when the ink presents a non-Newtonian response. Therefore, the ideal inks are those that have a low viscosity at higher shear rates when passing through the nozzle (i.e., shear thinning), and high enough viscosity at resting to provide good shape fidelity after being dispensed.[54,55] Thus, the printability

of the ink must be evaluated from two perspectives analyzing its ease to form a filament when extruded and its ability to keep the shape fidelity after deposition.

The experimental methodology developed in this section focuses on printability as the ability of the MRE ink to form a continuous filament with a diameter close to the nozzle one. To validate the method, we use as reference material a MRE ink composed of an extremely soft elastomeric matrix (stiffness ≈1 kPa after curing), and soft-magnetic particles with a mean diameter of 5 µm. Four different volume ratios of particles are considered, ϕ = 0%, 10%, 20%, 30% (see more details in Experimental Section). Note that each material (i.e., each particles volume ratio) presents different rheological properties over time so that they can be considered as four independent testing cases (see viscosity evolutions in **Figure 2**A). Because of these time-variations in the rheological properties of the inks, we hypothesize that there is an optimal print-window that favors the formation of filament during extrusion. This print-window is defined from the curing stage of the material when the viscous and elastic stress contributions reach an equilibrium allowing the filament formation, and the stage when the material solidifies impeding extrudability. Moreover, the ink must allow for constant flow rate or extrusion velocity during the printing avoiding inhomogeneous flows and irregular printed filaments. Taking all these features together, the pressure conditions needed for optimal DIW depend on the geometry of the extruder, the rheological properties of the ink and the extrusion speed. In addition, for reactive and non-Newtonian inks, this

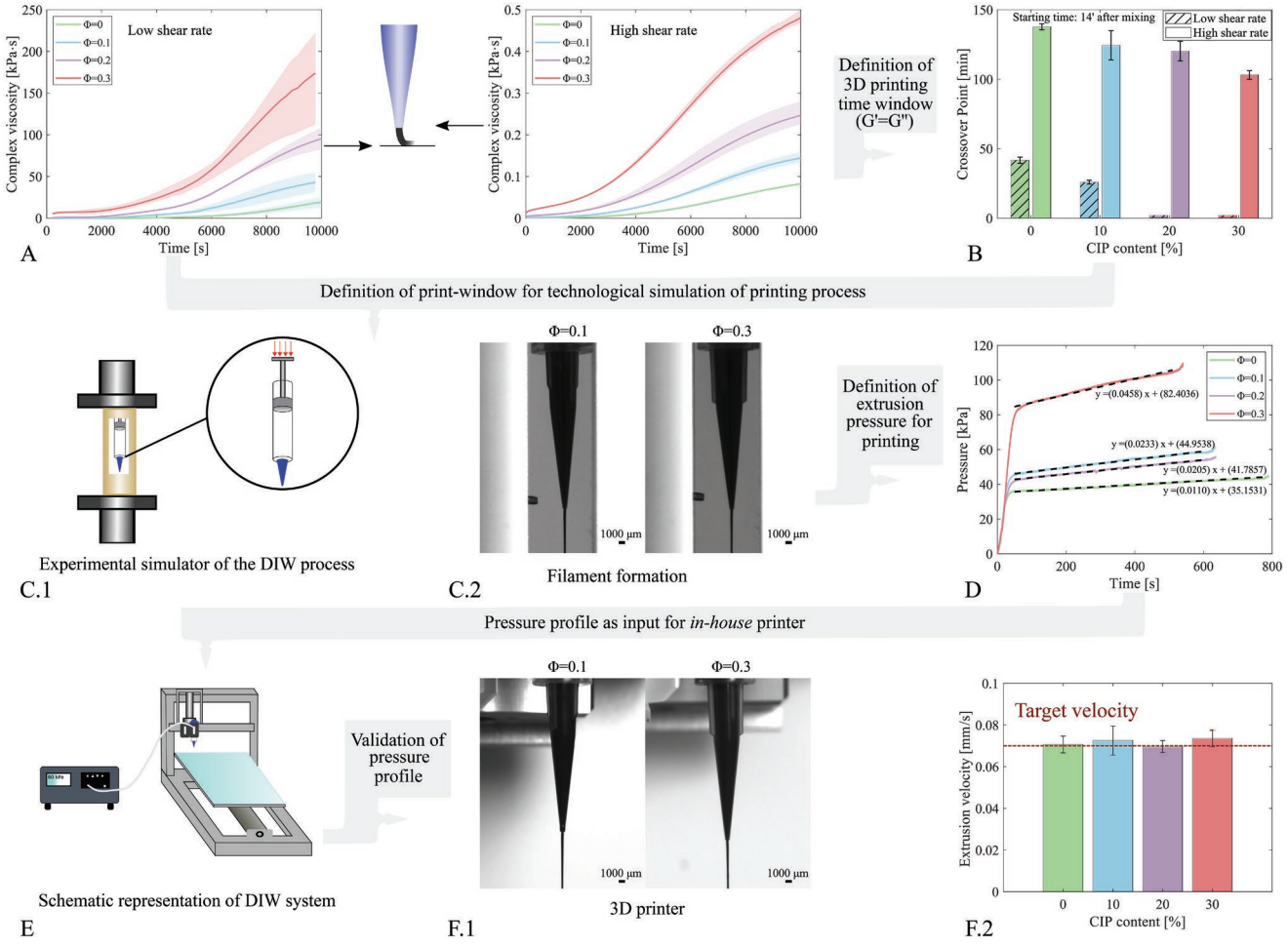

Figure 2. Experimental methodology to determine the print-window and ensure regular extrusion flow of reactive inks. A) Rheological characterization of MRE inks with different particles volume fractions of 0%, 10%, 20%, and 30% at low (0.03 rad s^{-1}) and high (30 rad s^{-1}) shear rate. These rate conditions are representative of the deposition and extrusion stages, respectively. B) Critical times for each MRE ink when the storage and loss moduli cross leading to solid-like behavior. These times, also known as crosslinked time, are computed for low and high shear rates and determine the temporal print-window. C) Experimental simulator of the DIW printing process based on compression tests: Scheme of the experimental setup (C.1); stable filament formation for a constant extrusion speed of 0.07 mm s^{-1}(C.2). D) Pressure profiles for each MRE ink, indicating the pressure needed over time to provide a constant extrusion speed of 0.07 mm s^{-1}. These profiles are given for a starting point equal to the crosslinked time identified in B for the lower shear rate. E) Scheme of the DIW system developed. F) Validation of the experimental methodology to provide regular filament formation: Filament formation in the DIW printer when applying the pressure profiles obtained in panel D for each MRE ink (F.1); comparison of the target extrusion speed (i.e., the speed imposed in the compression tests) with the mean extrusion velocity measured during the printing process using the pressure profiles obtained in panel D (F.2). In the panels, CIP content refers to the volume fraction of magnetic particles. Note that the error bars correspond to variations over time and between samples.

identification of optimal printing conditions is highly complex as the viscous response of the ink is affected by shear rate (so that by extrusion speed and tip geometry), and this dependence changes over printing time.

To overcome limitations associated to the need of several trial-error tests to identify optimal printing conditions depending on the material/ink used, we provide a multi-step experimental methodology. This method characterizes the rheological behavior of the ink and reproduces the desired printing process without the need of using the printer. Then, the outcome in the form of pressure profiles over time is provided to feed the printing system and to obtain robust filament conditions during the process. To start with, the ink is tested with a rheometer under oscillatory isothermal conditions and two different shear rates representative of the extrusion and deposition stages (see more details on the testing procedure in Experimental Section. The results from Figure S1, Supporting Information, motivate the choice of the two testing rates). These results for the four inks tested are shown in Figure 2A. This experiment allows to identify the lower bound of the print-window, defined by the time at which the storage (G′) and loss (G″) shear moduli cross (Figure 2B and Figure S2, Supporting Information). Note that this is the minimum time at which the material translates from a liquid-like to a solid-like behavior. This transition in material phase is essential to maintain the shape fidelity of the filament when deposited. However, this time may not be the optimal, as we discuss in the following section. Moreover, the upper bound limit that defines the temporal print-window coincides with the liquid-like to a solid-like behavior at the high shear rate experienced in the nozzle. This time corresponds to a significant decrease in ink flow that hinders further filament formation. Once the starting time for DIW is established, we need to define the pressure profile needed to provide consistent filament formation during time. To this end, we developed an experimental procedure that reproduces the printing process while evaluating the pressure profile when imposing a constant ink flow. The setup consists of a device that holds a cartridge filled with the ink and that is coupled to a universal testing machine (see Figure 2C, Figure S3, Supporting Information and further details in Experimental Section). Thus, the testing machine can be used in deformation-control mode to impose the desired ink flow (i.e., extrusion speed), and such a test provides the pressure needed to reach it. The pressure profiles for the four inks tested and for a desired extrusion velocity of 0.07 mm s^{-1} are provided in Figure 2D. We can appreciate how the pressure needed increases with time due to changes in the rheological properties of the ink. These pressure profiles can feed the in-house printer to ensure robust printing conditions over time independently of the property changes experienced by the ink (Figure 2E). This methodology is validated by comparing the filament formation obtained in the testing machine and in the printer, see Figures 2C.2 and 2F.2, respectively (see also Figure S4, Supporting Information). In addition, the method is validated by measuring the extrusion velocity in the printer over time. The results presented in Figure 2F.2 show that the proposed method is able to provide a constant extrusion velocity over time, which is almost identical to the target value. Note that these calculations are based on flow and gravimetrical analysis, and the error bars in Figure 2F.2 correspond to variations over time and between samples.

2.2. Hybrid Theoretical-Experimental Method for Robust Printability of Reactive Inks

The methodology presented in the previous section ensures a regular filament formation by identifying a print-window and the corresponding optimal evolution of the extrusion-pressure depending on the ink used. However, a robust printing process also requires a regular shape fidelity of the filament after deposition. Therefore, a further restriction of the print-window is needed to find the optimal printing conditions. Instead of choosing the starting printing time based on the liquid-like to solid-like transition, we identify a complex viscosity threshold. Note that such a material parameter, along with surface tension, is directly linked to the forces that determine the filament shape after deposition. The value found is equal to 12.9 kPa s and determines an optimal start-printing time of 115 and 60 min for MREs with 10% and 30% particle volume ratio, respectively (**Figure 3**A). These times are measured from the mixing of the polymeric phases with the filler content. Then, our in-house printer needs the definition of a pressure profile from this time to provide regular ink extrusion. This can be obtained experimentally from compression tests reproducing the printing process as explained above (see Figure 3C for experimental profiles). Alternatively to these experiments, we provide a computational method to estimate the evolution of the extrusion-pressure over printing. This method only requires standard rheological characterization and avoids more technological tests.

The computational method consists of a theoretical description of the printing process accounting for the geometry of the extruder and the rheological properties of the ink. From this information, the model provides an estimation of the pressure needed over time to obtain a constant flow rate, that is, extrusion speed. The constitutive description of the model is calibrated from rheological tests providing the dependence of material viscosity and shear stress on shear rate at different time points. Then, an analytical description of the extrusion process through the nozzle is used to estimate the profile of shear rates during filament extrusion. The constitutive model predicts the mechanical stress within the material extruded and provides a final relationship between the pressure applied in the cartridge and the extrusion speed. In Figure 3B we show the constitutive calibration for two MRE precursors (10% and 30% particle volume fractions) and, in Figure 3C we present the pressure estimations from the complete model. In this regard, the computational method presented provides a good estimation of the temporal evolution of extrusion-pressure during printing accounting for the evolving changes in the rheological properties of the ink. The 10% MRE ink presents a more complex behavior due to the longer time to reach the target viscosity threshold and, as a consequence, a higher curing stage. This higher complexity impacts the model predictions and leads to larger errors. Further details on the model description and implementation can be found in Experimental Section.

To validate the appropriateness of the hybrid theoretical-experimental method, we evaluate it for the two different materials, that is, MRE precursors with 10% and 30% particle volume fractions. To this end, we feed our in-house printer with the pressure profiles computed from the theoretical

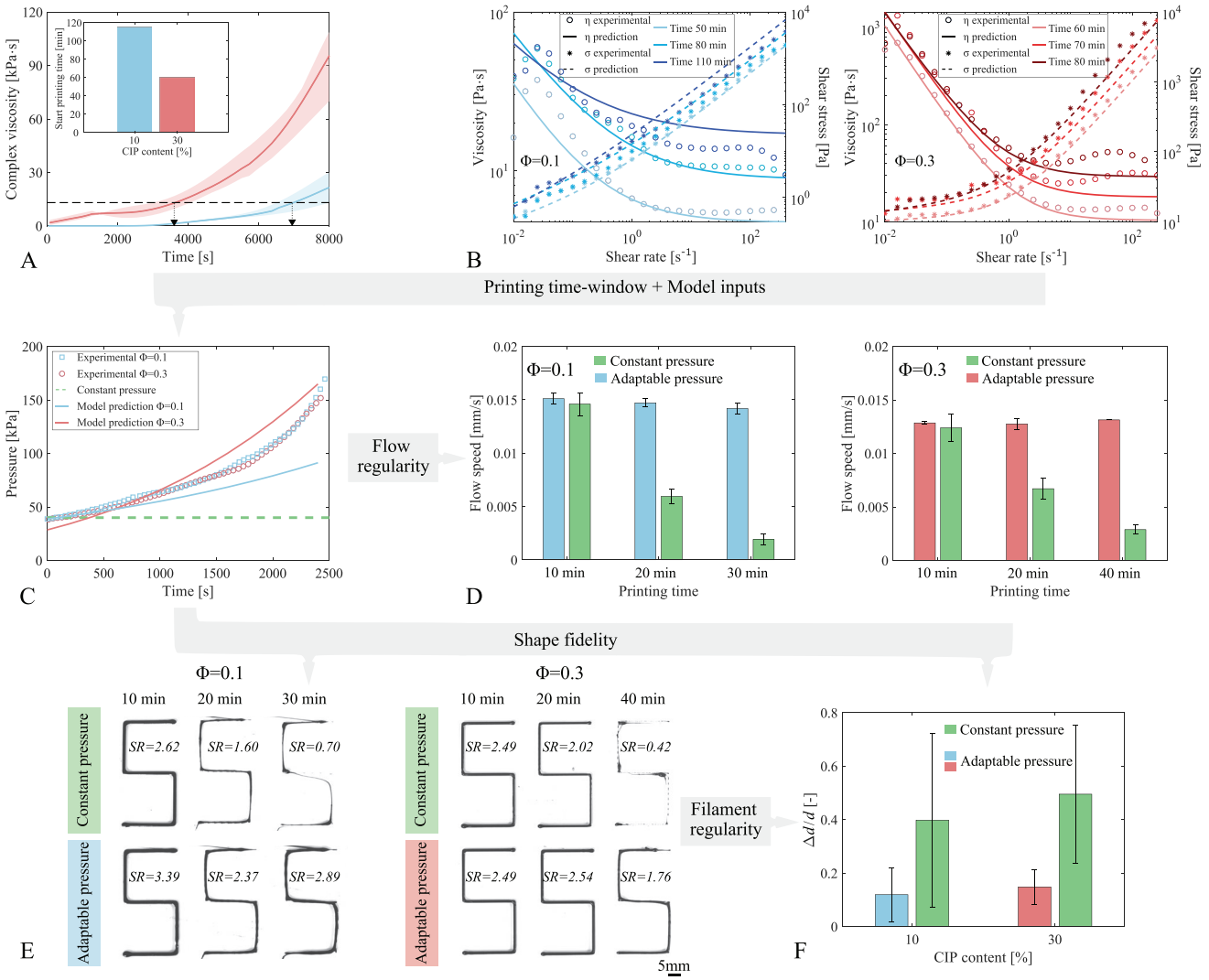

Figure 3. Hybrid theoretical-experimental methodology to print reactive inks. A) Rheological characterization of MRE inks with different particles volume fractions of 10% and 30% at low shear rate. Identification of the optimal start-printing time from a critical (empirical) complex viscosity threshold. B) Comparison between experimental results and model predictions of viscosity and shear stress versus shear rate at different time points. The left panel shows the results for 10% MRE and the right panel shows the results for 30% MRE. C) Experimental pressure profiles for each MRE ink, indicating the pressure needed over time to provide a constant extrusion speed of 0.015 mm s^{-1}. The theoretical model predictions are plotted for both MRE inks, as well as a constant pressure profile. These adaptable and constant extrusion-pressure profiles are used in the following tests. D) Validation of the methodology by comparing the extrusion speed over time using the adaptable and constant pressure profiles obtained in panel C for (left) 10% MRE and (right) 30% MRE. E) Images of the S-shape tests and associated spreading ratio (SR) over time using the adaptable and constant pressure profiles obtained in panel C for (left) 10% MRE and (right) 30% MRE. The SR is computed from the horizontal filament in the middle of the S-shape. F) Analysis of filament width' regularity represented as the ratio of the thickness deviation into mean thickness over time for 10% and 30% MREs.

model. Moreover, we consider two printing technologies for comparison in all the validation tests, that is, a temporally adaptable extrusion-pressure (our approach) and a constant extrusion-pressure (standard approach). First, a comparison in terms of flow rate regularity is performed, Figure 3D. The target extrusion speed chosen was reduced with respect to the previous analysis to better adapt it to printing conditions when complex shapes are required. A regular flow speed over time is obtained when employing our evolving-pressure approach whereas an important loss in speed flow is observed when applying a constant extrusion-pressure. These results clearly demonstrate an advantage of our method with respect to standard printing technologies, for the two materials tested. In addition, we evaluate the method not only to provide a regular filament formation but also a good filament shape fidelity after material deposition. These results are shown in Figure 3E in terms of S-shape printing tests. These tests have a double purpose: the evaluation of deposited filament width, and the capability of the in-house printer to faithfully capture abrupt changes in printing direction over time. This figure presents a comparison between using adaptable extrusion-pressure and a constant extrusion-pressure. Similarly to flow speed evolution during printing, these results show a clear advantage of our adaptable approach with respect to standard technologies.

The mean spreading ratio (SR) provided is equal to 2.88 and 2.26 for MREs with 10% and 30% particle volume ratio, respectively. Furthermore, an analysis of regularity of the filament width is shown in Figure 3F, represented as width deviation into mean width over time. The results demonstrate once more a superior performance of our approach. The printing resolution of the system for different inks is evaluated in terms of filament width and layer thickness. The results are presented in Figure S6, Supporting Information and, for the MRE inks, show an optimal resolution of 390 and 136.5 μm in filament width and height, respectively. Indeed, our proposed methodology not only allows for regular printing conditions but also for widening the print-window and, therefore, the possibility to manufacture bigger structures.

2.3. Temporal-Updated Direct Ink Writing Enables the Printing of Soft MREs and Conductive Materials for Applications in Mechanobiology and Soft Electronics

The theoretical-experimental methodology presented enables the robust printing of soft multifunctional materials, even when reactive inks are used. This technology opens interesting possibilities for different fields such as biomedical engineering and soft electronics. Here, we demonstrate the applicability of this DIW approach to two challenges: 1) the printing of multi-compartment MREs as substrates for cellular stimulation; and 2) the printing of deformation sensors based on conductive elastomers.

Prior to addressing these problems, we evaluate the quality of the printed samples by means of multifunctional performance. To this end, we print cylindrical samples of 20 mm diameter and 1 mm height for magneto-rheological testing under shear loading. The samples are manufactured with 30% MRE and they are printed at different time points within the identified print-window: 0, 20, and 35 min. The results by means of shear stress versus shear strain, and at different applied magnetic fields of 0, 200, and 500 mT, are shown in **Figure 4**A. The multifunctional behavior of the samples is very regular demonstrating a robust printability not only in terms of shape fidelity but also in terms of multi-physics behavior. Furthermore, the magneto-mechanical response of the printed samples is almost identical to the response of samples manufactured using molding techniques (see corresponding results in our previous publication).[44]

The first application is motivated by a recent work by the authors that demonstrates the potential of brain-like soft MREs as biological substrates to transmit dynamic forces to cellular systems.[17] In that work, the authors developed a magneto-mechanical system that allows for the generation of complex magnetic conditions within an effective region where the MRE sample is placed. These magnetic fields interact with the particles embedded into the MRE leading to dipole–dipole interactions that result into the macroscopic deformation of the sample (see Figure 4B.2). The MRE substrates are functionalized so that biological cells can be cultured on the surface. Therefore, the system enables the non-invasive and dynamic actuation on the cells by transmitting forces and deformation from the active substrate via external magnetic stimuli. The main limitation of such a stimulation framework is that the addition of magnetic particles makes the substrate opaque, so that the system is limited to upright fluorescence microscopy. However, the possibility of printing multi-compartment samples using different materials allows for manufacturing substrates composed of MRE inks with a high particle content in the peripheral region, and transparent elastomeric inks within the central region. This way the system can be used in most of the standard microscopes including inverted ones. We test the capability of our DIW approach to produce these multi-material samples printing cylinders with a total height of 4 mm and an external diameter of 20 mm. These samples are composed of 30% MRE and, in the central region delimited by 8 mm diameter, of 0% MRE (i.e., pure elastomeric matrix). The manufacturing of the samples is possible by coupling two cartridges (each one with a different ink) to two independent pressure-controllers, see Figure 4B.1. A good printability and shape fidelity is obtained, see Figure 4B.2. After printing, the sample is functionalized and human-dermal fibroblasts are cultured on top (see further details in Experimental Section). An efficient transmission of magneto-mechanical forces from the printed sample to the cells can be appreciated in Figure 4B. This figure panel presents the same set of fibroblasts before and after stimulation, showing a significant stretching of the cells when the magnetic stimulus is applied.

The second application consists in the DIW printing of a soft conductive material on a flexible beam (**Figure 5**A). The ink used is composed of the same elastomeric matrix used for the MRE inks but filled with conductive particles (see Experimental Section for further details on materials and ink preparation). Prior to printing, rheological characterization and compression tests simulating the DIW process were conducted (Figure S7, Supporting Information). These tests provide the print-window and the pressure profile needed in our in-house printer for consistent filament formation and shape fidelity over time. Then, a U-shape filament structure composed of two-layers with a total height of 1 mm was printed on the beam. This disposition allows for connecting two electrodes on one side of the beam, which is clamped. The other side of the beam is joined to a uniaxial testing machine to impose controlled displacements on its vertical direction leading to bending. When the beam is bended, the soft printed structure is deformed in a tension-like or compression-like manner (see Figure 5C). The electric resistance of the sensor is determined by the conductivity of the printed material that, in turn, is directly related to the formation of conductive pathways formed by the embedded particles. Therefore, the bending actuation can either promote compression states that favor conductivity decreasing the sensor resistance; or, on contrary, can promote tension states that hinder conductivity increasing the sensor resistance (see Figure 5B).

3. Discussion and Conclusion

The development of soft multifunctional materials is currently experiencing a great advance with the addition of programmed mechanical responses to external stimuli. The characterization of these materials usually requires simple geometries that can be easily obtained by molding techniques or other

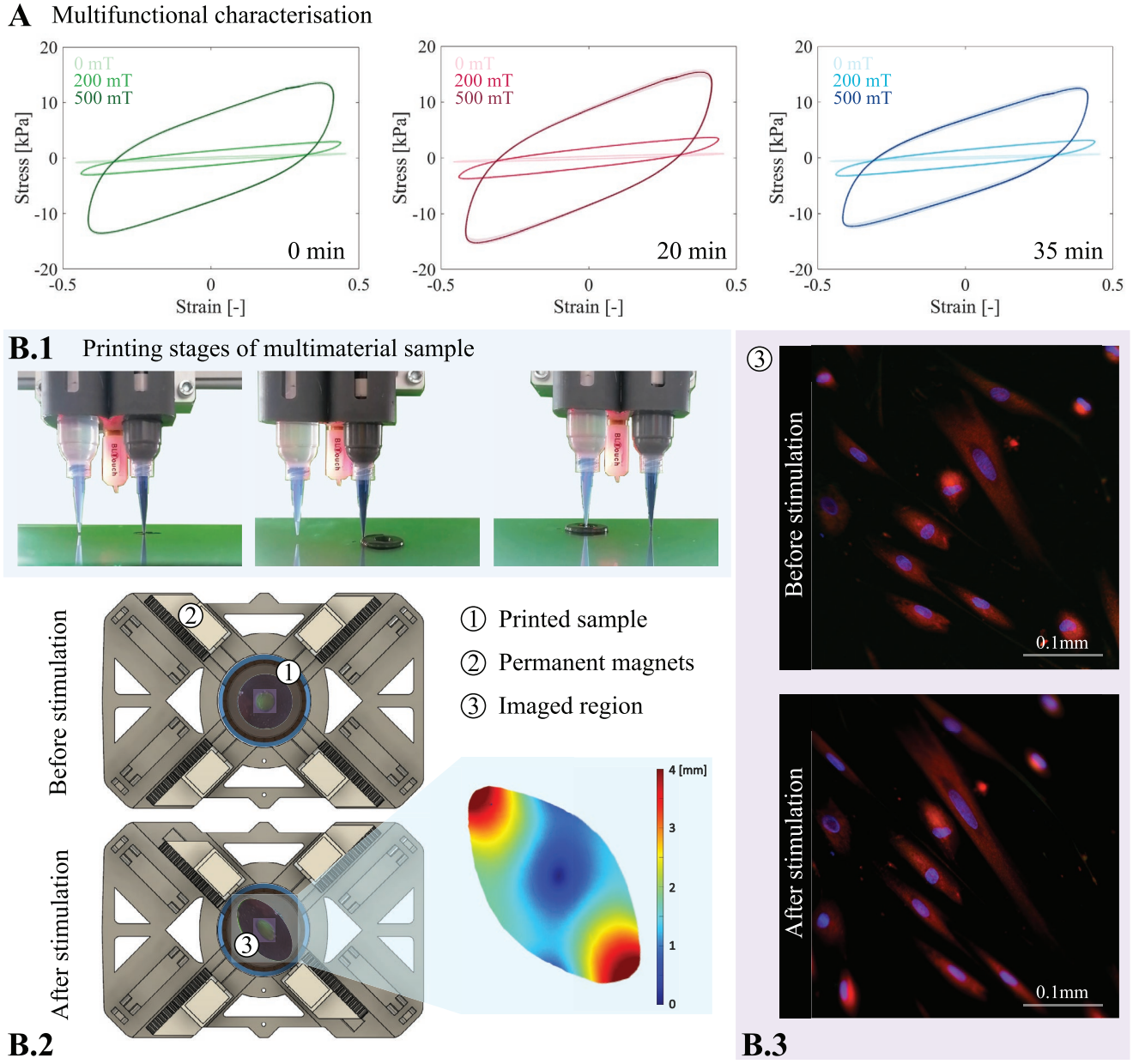

Figure 4. Temporal-updated DIW allows to manufacture magneto-active materials for biological stimulation. A) Magneto-rheological characterization under shear loading of 30% MRE-cylindrical samples manufactured at different printing times: (left) starting print-time; (middle) 20 min printing time; (right) 35 min printing time. The results show a regular behavior independently of the printing time used, when the temporal-updated DIW approach is employed. The shaded region represents the error dispersion from three repetitions per test condition. B) DIW printing and application of magneto-active substrates for biological stimulation. DIW stages of the printing process of multi-material samples using at once 0% and 30% MREs for different regions (B.1). Magneto-mechanical stimulation device[17] based on permanent magnets (2) to activate the mechanical deformation of the printed MRE sample (1), and displacement fields obtained from digital image correlation on the printed sample (B.2). Microscopic images of a set of human dermal fibroblasts cultured in a local region of the MRE sample ((3) in panel B.2) before and after magneto-mechanical stimulation (B.3). A significant stretch on the fibroblast in observed after stimulation. The cell nuclei are marked in blue, the cytoskeleton in green and mitochondria in red.

traditional manufacturing methods. These fundamental works are providing a deep understanding of the underlying physics governing their multifunctional response. In parallel to such characterization works, different authors are advancing on the formulation and implementation of constitutive multi-physics models within advanced computational frameworks.[9,56] Although these numerical tools enable the virtual testing of complex structures to address real problems in different engineering fields, their manufacturing encounters critical issues. The geometrical limitations can be eventually overcome by using additive manufacturing techniques. However, the robust printing of reactive inks whose rheological properties significantly evolve over time is still challenging. Previous solutions proposed the inclusion of additives to enhance the printability

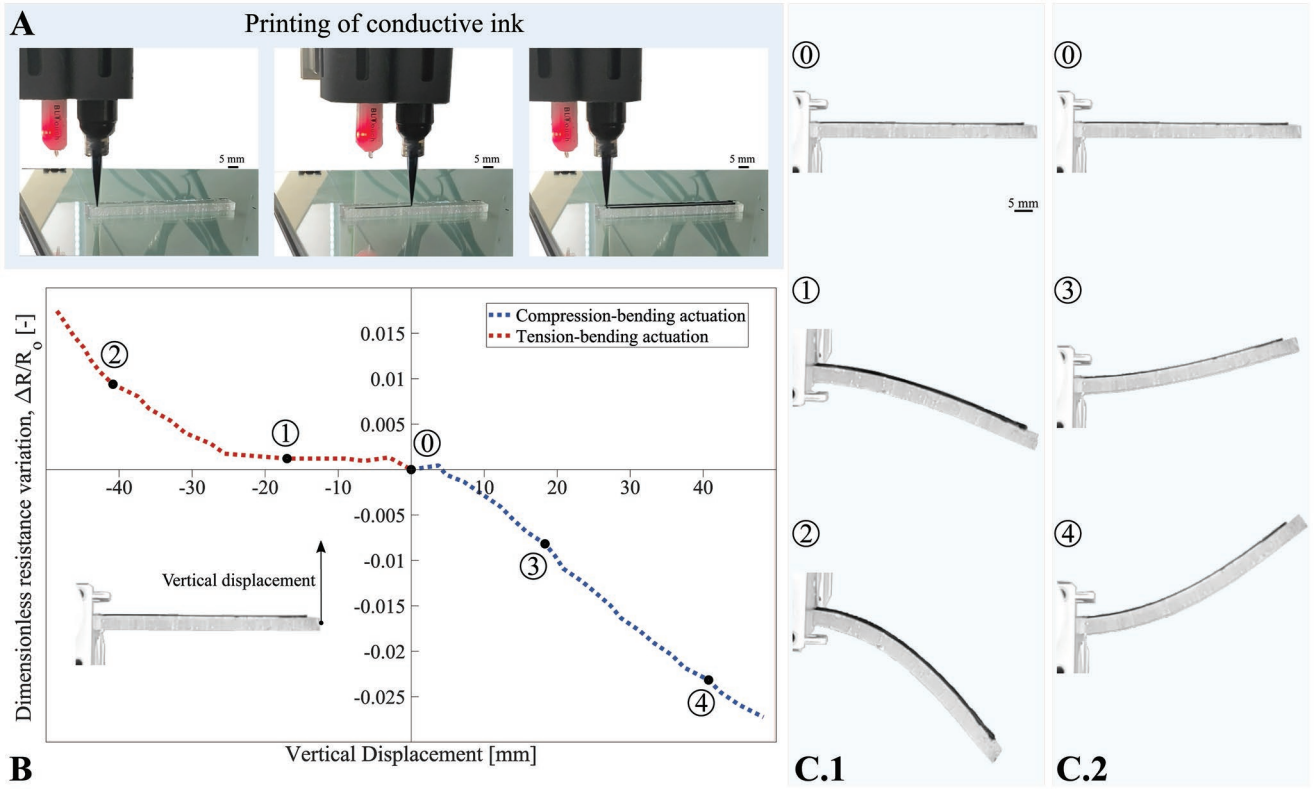

Figure 5. Temporal-updated DIW allows to manufacture conductive materials for soft electronics. A) DIW stages of the printing process of conductive elastomer on a flexible beam. B) Dimensionless variation of the electric resistance in the printed sample when the beam is bended. The variation of resistance is provided against the vertical displacement of the beam differentiating between compression-bending actuation and tension-bending actuation. C) Experimental images of the functionalized beam during the bending actuation corresponding to the points highlighted in panel B for: tension-bending actuation (C.1); compression-bending actuation (C.2).

of the material or the combination of different elastomeric matrices. To this end, fumed silica nanoparticles or a polymerization retardant (e.g., Slo-Jo) are added to the ink.[18,24,49,50] Although these approaches are extremely valuable, they do not keep the matrix and filler phases intact. In this work, we address these printing limitations by introducing a temporal-updated DIW methodology. This method consists in a hybrid experimental–theoretical framework that, depending on the specific ink, provides the optimal printing conditions over time. These optimal conditions can be straightforwardly input in the open-software in-house DIW printer developed in this work. The method enables the printing of multifunctional materials traditionally manufactured by molding techniques straightforwardly, without changing their final material response as demonstrated in Figure 4 for MRE samples. This point represents an important advantage as these materials have been found as excellent candidates for biomedical and soft robotics/electronics applications.[9,17] In this regard, note that previous approaches printed materials with a final stiffness in the order of 10^2–10^3 kPa, whereas we provide multifunctional materials with brain-like stiffness (≈1 kPa).

Along the work, the complete methodology has been satisfactorily tested for printing different soft multifunctional materials (stiffness of 1–10 kPa), that is, different MREs and a conductive elastomeric composite. In addition, we have validated the method with two challenging applications: the development of multicompartment MREs for mechanobiology experimentation; and the manufacturing of electro-mechanical sensors. Overall, the results show a robust printability within a printing time-window that can be identified from standard rheological tests. The current approach thus allows for printing multifunctional structures with a resolution of 136.5–188.1 μm in layer thickness, 255–390 μm in filament width (depending on the ink tested and nozzle used, see Figure S6, Supporting Information), and a sample height of at least 5 mm (maximum height tested). Further considerations for improvement will make use of the heating bed of the printer and the possibility of controlling temporal variations of the bed temperature during the manufacturing process. Preliminary tests suggest a great potential in shape fidelity and reachable heights, as the increase in temperature accelerates the curing process of the deposited material. Additional rheological tests at different testing temperatures will provide the evolution of ink viscosity and shear moduli during curing under alternative thermal conditions. Regarding the theoretical model, the constitutive formulation can be easily extended to incorporate thermal dependences and to capture more faithfully the geometrical problem. In this regard, the extrusion process may be implemented within a finite element framework to account for spatial dependences and gradients in shear rate or temperature. Furthermore, a second stage modeling framework could be developed to reproduce not only the extrusion process but also the filament deposition and inter-filament adhesion.

This new method may open new routes in the development of multifunctional materials that can interact with biological tissues or that can be integrated in soft robotic components. Direct applications may relate to multi-material magneto-responsive structures that can change stiffness and mechanical deformation forming heterogeneous patterns. These will provide great opportunities for mechanobiology testing allowing to create dynamic heterogeneous changes in cellular substrate properties mimicking pathological conditions such as tissue scarring. Other potential applications for magneto-responsive materials are extremely soft structures that can mechanically respond to very low magnetic fields. Note that the mechanical actuation directly depends on the mechanical balance between the MRE stiffness and the induced magnetic stress. Therefore, the possibility to manufacture complex multi-material structures with very low heterogeneous stiffnesses (≈1–10 kPa) enables magnetic actuation with small external fields. Moreover, this technology also opens the use of reactive inks for soft conductive composites. Hence, it allows to create complex conductive patterns whose electric conductivity continuously changes with mechanical deformation. The latter enables the design of electro-mechanical sensor systems to reconstruct temporal deformation processes from the recorded electric signals. Finally, it is worth to mention that the proposed technology is not limited to these materials but may be used for the design of other multifunctional structures suitable for DIW.

4. Experimental Section

In-House DIW Printer Description: An in-house DIW printer designed as a motorized cartesian-XZ-Head gantry (see Figure 1 and Supporting Information) was developed herein. The remaining Cartesian coordinate Y was controlled by the bed movement. The printer incorporated a heated bed with a temperature range up to 80 °C and two extruders that allowed multi-material patterning and deposition. The extrusion of each material was driven by an independent pressure controller (Ultimus V, Nordson, USA). The controller delivered air pressure to a cylindrical cartridge and produced material flow from the cartridge to the printing bed through a conical dispensing tip. Pressure controllers had multiple memory cells, each of one with configurable pressure loads and dispensing times. Additionally, the controller features an auto-increment mode that allowed the user to run a sequence of timed dispense cycles stored in different memory cells. This granted the capability of adjusting the dispensing parameters over the printing process to overcome material changes on the dispensing cartridge whether the material was being printed or not, since the pressure controller could operate independently from the 3D printer.

A modified version of Marlin, an open-source firmware for 3D printers, was used to control all the actuators and interpret GCODE files generated by standard slicer software (e.g., Ultimaker Cura). Customized GCODE command libraries had been designed to perform serial communication between the 3D printer and the pressure controllers to regulate initiation, evolution, and interruption of the flow during the printing process. Automatic inclusion of these flow control commands in standard GCODE files was done by means of a text-editing script in MATLAB. This modified GCODE file contained all the necessary commands to 3D print a time-evolving material with a pressure-driven extrusion system.

Preparation of Pre-Crosslinked Inks Formulations: The MREs-based inks were composed of an elastomeric matrix and soft magnetic particles. The matrix consisted of DOWSIL CY 52-276 polydimethylsiloxane (PDMS) from Dow (Dowsil, Midland, MI, USA), provided as a two-component formulation with part A and B which were mixed in equal mass ratio. The magnetic particles used correspond to soft SQ carbonyl iron powder (CIP) (BASF, Germany) with a mean diameter of 3.9 – 5 mm. Three ink-formulations based on the bi-component PDMS mixed with four CIP volume fractions (0, 10, 20, and 30 vol%) were prepared. Moreover, the conductive ink consisted of the same PDMS matrix filled with carbon black particles with a mean diameter of 50 nm (Vulcan XC72r) (Cabot Corporation, Boston, USA) with a volume fraction ratio of 10%. All components were mixed manually until complete homogenization at room temperature. Moreover, the mixture was loaded into a syringe and extruded through a smooth-flow tapered tips (22G, 0.41 mm internal diameter) (Nordson, Westlake, OH; USA) to remove all possible aggregates associated to particle–particle interactions. Finally, the sample was degassed under vacuum for about 10 min.

Rheological Characterization: The rheological properties of the inks were measured with a TA-HR-20 rheometer (TA instruments, New Castle, DE, USA) at 25 °C. All experiments were performed using a parallel plate geometry of stainless steel with a 40 mm diameter. The evaluation of curing inks profiles was determined by oscillatory test under isothermal conditions (25 °C) at a constant amplitude (1% strain) and at two different frequencies (0.03 and 30 rad s^{-1}). The gap selected was 1 mm. The crosslinked time was determined with TRIOS v5.1.1.4 software at the crossover point ($G' = G''$). Shear rate sweeps were performed by varying the shear rate from 0.01 to 500 s^{-1} using a gap of 0.5 mm. Those experiments were performed at different curing times for each ink to determine the evolution of the consistency index and flow index with time. All experiments were performed considering at least three replicates.

Experimental Simulator of the DIW Printing Process: This method allowed to obtain the evolution of pressure over time through mechanical compression tests that simulate the extrusion process in the 3D printer. A testing device was designed and manufactured by fused deposition modeling to hold the syringe containing the ink. This device was coupled to a universal testing machine (Instron 34TM-5), with a load cell of 50 N. Note that a load cell of 5 kN was used for the tests on conductive inks, as these reached higher compressive forces. The upper compression plate applied force through a plunger rod to drive the fluid to the desired extrusion speed, while the lower one was fixed. The measured force over time was that required to keep the plunger moving while maintaining a constant flow rate through the needle.

Experimental Procedure to Evaluate Material Printability: Zigzag patterns were performed by filament deposition with a layer height of 0.5 mm. Different printing speeds (800, 1000, 1200, and 1400 mm s^{-1}) were tested with both a constant pressure (reduction of the flow with time) and with the pressure profile obtained from the theoretical model (Figure S5, Supporting Information). The last condition ensured a constant flow rate. Images of the filament were photographed with a DIC camera along with a ruler which later served as reference system. To measure the printing filament diameter, photographs were processed with ImageJ software (ImageJ, U.S. National Institutes of Health, Bethesda, MD, USA). The optimal printing condition was determined according to the spreading ration (SR) as printing filament diameter into nozzle diameter.

Magneto-Mechanical Characterization of MRE Printed Samples Under Shear Loading: The magneto-mechanical behavior of the 3D printed MRE specimens was studied under a constant oscillatory shear following the same approach as in previous work by the authors.[44] The previously described rheometer was used in these experiments but with a specific magneto-rheological peltier able to set a magnetic field in the axial direction to the sample. The homogeneous field was ensured by an upper yoke. A parallel plate geometry made of low magnetic permeability stainless steel with a 20 mm diameter and a gap of 1 mm was used. Further description of the system could be found in Moreno et al.[44] Oscillatory sweep tests at a constant strain (48%) and fixed angular speed of 0.9 rad s^{-1} were carried out under different magnetic flux densities (B = 0, 200, and 500 mT). All experiments were performed considering at least three replicates.

Computational Model: The model predicted the pressure drop of a fluid subjected to simple shear in a tapered nozzle. The model formulation followed the procedure reported in ref. [57] but described the flow behavior by a Sisko model (non-Newtonian model). For a differential of length, ∂l, subjected to forces to the centre line, the force balance reads:

$$\partial P \pi r^2 = 2\pi r \partial l \sec\theta \sigma \cos\theta$$
$$\partial P = \frac{2\sigma}{r}\partial l \quad (1)$$

where ∂P is the differential of pressure, σ is the shear stress, and the radius of the tip is defined as $r = r_1 + l\tan\theta$, with θ being half the angle cone and r_1 the smallest radius of the tip (see Figure S8, Supporting Information). Therefore, we could define $\partial l = \partial r/\tan\theta$. The Sisko model for the shear stress is expressed as

$$\sigma = K\dot{\gamma}^n + \eta_\infty \dot{\gamma} \quad (2)$$

Since the flow behavior of the material changes over time, here, the consistency parameter K, the power law index n, and the infinite viscosity η_∞ were time-dependent. The shear rate could be defined as $\dot{\gamma} = \frac{4Q}{\pi r^3}$, where $Q = \pi R^2 \nu$ is the volume of flow rate, R is the cartridge radius, and ν the velocity of the "stopper." This flow model considered an infinite shear viscosity plateau at high shear rates. Combining Equation (1) with the definition of ∂l and Equation (2), the differential pressure is written as

$$\partial P = \frac{2}{\tan\theta}\left[K\left(\frac{4Q}{\pi r^3}\right)^n + \eta_\infty\left(\frac{4Q}{\pi r^3}\right)\right]\frac{\partial r}{r} \quad (3)$$

Then, integrating over the maximum and minimum radii of the tip, the inlet pressure is obtained as:

$$P = \frac{2}{3\tan\theta}\left[\frac{K}{n}\left(\frac{4Q}{\pi}\right)^n\left(\frac{1}{r_1^{3n}} - \frac{1}{r_0^{3n}}\right) + \eta_\infty\left(\frac{4Q}{\pi}\right)\left(\frac{1}{r_1^3} - \frac{1}{r_0^3}\right)\right] \quad (4)$$

Further details on the model formulation and implementation can be found in Supporting Information.

Cell Culture: Human dermal fibroblasts were used to assess the potential of the 3D-printed MRE samples for mechanobiology studies. Cells were cultured in DMEM (Gibco, Fisher Scientific, USA), supplemented with 10% FBS (Sigma-Aldrich, USA), 100 IU mL^{-1} penicillin and 100 IU mL^{-1} streptomycin (Gibco, Fisher Scientific, USA), in a humidified CO_2 incubator at 37 °C. For individual cell imaging, fibroblasts were seeded at low-density (7×10^3 cells cm^{-2}) on the MRE, previously coated with a 0.1 mg mL^{-1} collagen solution (Gibco, Fisher Scientific, USA) under UV exposure for 2 h to enhance substrate biocompatibility. Morphological analysis was performed 24 h after seeding. Fibroblasts were incubated for 1 h with NucBlue Live Cell Stain (Invitrogen, Fisher Scientific, USA) for nuclei staining (blue), BioTracker 488 Green Microtubule Cytoskeleton Dye (Sigma-Aldrich, USA) for cytoskeleton staining (green) and MitoTracker Red CMX-Ros (Invitrogen, Fisher Scientific, USA) for mitochondria staining (red), following manufacturers' instructions. After labeling removal, fresh culture medium, with no phenol red, was added. Subsequently, fibroblasts were imaged with an upright fluorescence microscope Leica DM6 B (Leica Microsystems, Wetzlar, Germany) and a 20× water-dipping objective, in a humidified incubation chamber at 37 °C and 5% CO_2, before and after magneto-mechanical actuation.

Supporting Information

Supporting Information is available from the Wiley Online Library or from the author.

Acknowledgements

M.L.L.-D., G.d.A.-I., and S.G.-H. contributed equally to this work. The authors acknowledge support from the European Research Council (ERC) under the European Union's Horizon 2020 research and innovation programme (grant agreement No. 947723, project: 4D-BIOMAP). The authors acknowledge support from Programa de Apoyo a la Realizacion de Proyectos Interdiscisplinares de I+D para Jovenes Investigadores de la Universidad Carlos III de Madrid and Comunidad de Madrid (project: BIOMASKIN). DGG acknowledges support from the Talent Attraction grant (CM 2018 - 2018-T2/IND-9992) from the Comunidad de Madrid.

Conflict of Interest

The authors declare no conflict of interest.

Data Availability Statement

The data that support the findings of this study are available from the corresponding author upon reasonable request.

Keywords

4D printing, conductive elastomers, direct ink writing, magnetorheological elastomers, multifunctional materials

Received: October 24, 2022
Published online: December 23, 2022

[1] E. Yarali, M. Baniasadi, A. Zolfagharian, M. Chavoshi, F. Arefi, M. Hossain, A. Bastola, M. Ansari, A. Foyouzat, A. Dabbagh, M. Ebrahimi, M. J. Mirzaali, M. Bodaghi, *Appl. Mater. Today* **2022**, *26*, 101306.
[2] Y. Wu, X. Dong, J. kang Kim, C. Wang, M. Sitti, *Sci. Adv.* **2022**, *8*, eabn3431.
[3] L. Wang, D. Zheng, P. Harker, A. B. Patel, C. F. Guo, X. Zhao, *Proc. Natl. Acad. Sci. U. S. A.* **2021**, *118*, e2021922118.
[4] Y. Kim, E. Genevriere, P. Harker, J. Choe, M. Balicki, R. W. Regenhardt, J. E. Vranic, A. A. Dmytriw, A. B. Patel, X. Zhao, *Sci. Rob.* **2022**, *7*, eabg9907.
[5] M. B. Akolpoglu, Y. Alapan, N. O. Dogan, S. F. Baltaci, O. Yasa, G. A. Tural, M. Sitti, *Sci. Adv.* **2022**, *8*, eabo6163.
[6] U. Bozuyuk, E. Suadiye, A. Aghakhani, N. O. Dogan, J. Lazovic, M. E. Tiryaki, M. Schneider, A. C. Karacakol, S. O. Demir, G. Richter, M. Sitti, *Adv. Funct. Mater.* **2022**, *32*, 2109741.
[7] S. Lucarini, M. Hossain, D. Garcia-Gonzalez, *Compos. Struct.* **2022**, *279*, 114800.
[8] A. K. Bastola, M. Hossain, *Mater. Des.* **2021**, *211*, 110172.
[9] M. A. Moreno-Mateos, M. Hossain, P. Steinmann, D. Garcia-Gonzalez, *npj Comput. Mater.* **2022**, *8*, 162.
[10] M. Bahreman, N. Arora, H. Darijani, S. Rudykh, *Eur. J. of Mech., A: Solids* **2022**, *94*, 104534.
[11] M. Rambausek, D. Mukherjee, K. Danas, *Comp. Methods Appl. Mech. Eng.* **2022**, *391*, 114500.
[12] D. Mukherjee, K. Danas, *Int. J. Solids Struct.* **2022**, *257*, 111513.
[13] D. Garcia-Gonzalez, T. Ter-Yesayants, M. A. Moreno-Mateos, M. L. Lopez-Donaire, *Composites, Part B* **2023**, *248*, 110357.
[14] M. Cianchetti, C. Laschi, A. Menciassi, P. Dario, *Nat. Rev. Mater.* **2018**, *3*, 143.

[15] J. D. Kiang, J. H. Wen, J. C. del Álamo, A. J. Engler, *J. Biomed. Mater. Res., Part A* **2013**, *101A*, 2313.
[16] F. E. Uslu, C. D. Davidson, E. Mailand, N. Bouklas, B. M. Baker, M. S. Sakar, *Adv. Mater.* **2021**, *33*, 2102641.
[17] M. A. Moreno-Mateos, J. Gonzalez-Rico, E. Nunez-Sardinha, C. Gomez-Cruz, M. L. Lopez-Donaire, S. Lucarini, A. Arias, A. Muñoz-Barrutia, D. Velasco, D. Garcia-Gonzalez, *Appl. Mater. Today* **2022**, *27*, 101437.
[18] Y. Kim, H. Yuk, R. Zhao, S. A. Chester, X. Zhao, *Nature* **2018**, *558*, 274.
[19] Z. Liu, M. Li, X. Dong, Z. Ren, W. Hu, M. Sitti, *Nat. Commun.* **2022**, *13*, 2016.
[20] L. Brusa da Costa Linn, K. Danas, L. Bodelot, *Polymers* **2022**, *14*, 9.
[21] H. Li, S. Wang, X. Dong, X. Ding, Y. Sun, H. Tang, Y. Lu, Y. Tang, X. Wu, *Nano Energy* **2022**, *101*, 107585.
[22] Z. Zhu, D. W. H. Ng, H. S. Park, M. C. McAlpine, *Nat. Rev. Mater.* **2021**, *6*, 27.
[23] S. Wu, J. Eichenberger, J. Dai, Y. Chang, N. Ghalichechian, R. R. Zhao, *Adv. Intell. Syst.* *4*, 2200106.
[24] H. Yuk, X. Zhao, *Adv. Mater.* **2018**, *30*, 1704028.
[25] Y. Cheng, K. H. Chan, X.-Q. Wang, T. Ding, T. Li, X. Lu, G. W. Ho, *ACS Nano* **2019**, *13*, 13176.
[26] S. Bodkhe, P. Ermanni, *Eur. Polym. J.* **2020**, *132*, 109738.
[27] X. Kuang, S. Wu, Q. Ze, L. Yue, Y. Jin, S. M. Montgomery, F. Yang, H. J. Qi, R. Zhao, *Adv. Mater.* **2021**, *33*, 2102113.
[28] B. Yao, L. Scalcode Vasconcelos, Q. Cui, A. Cardenas, Y. Yan, Y. Du, D. Wu, S. Wu, T. K. Hsiai, N. Lu, X. Zhu, X. He, *Mater. Today* **2022**, *53*, 84.
[29] M. A. S. R. Saadi, A. Maguire, N. T. Pottackal, M. S. H. Thakur, M. M. Ikram, A. J. Hart, P. M. Ajayan, M. M. Rahman, *Adv. Mater.* **2022**, *34*, 2108855.
[30] N.-B. Cho, T.-H. Lim, Y.-M. Jeon, M.-S. Gong, *Sens. Actuators, B* **2008**, *130*, 594.
[31] F. H. Mostegel, M. Roth, M. Gassner, A. Oesterreicher, R. Piock, M. Edler, T. Griesser, *Prog. Org. Coat.* **2016**, *94*, 116.
[32] K. Chen, L. Zhang, X. Kuang, V. Li, M. Lei, G. Kang, Z. L. Wang, H. J. Qi, *Adv. Funct. Mater.* **2019**, *29*, 1903568.
[33] L. J. Tan, W. Zhu, K. Zhou, *Adv. Funct. Mater.* **2020**, *30*, 2003062.
[34] D.-H. Kim, N. Lu, R. Ma, Y.-S. Kim, R.-H. Kim, S. Wang, J. Wu, S. M. Won, H. Tao, A. Islam, K. J. Yu, T. il Kim, R. Chowdhury, M. Ying, L. Xu, M. Li, H.-J. Chung, H. Keum, M. McCormick, P. Liu, Y.-W. Zhang, F. G. Omenetto, Y. Huang, T. Coleman, J. A. Rogers, *Science* **2011**, *333*, 838.
[35] T. J. Wallin, J. Pikul, R. F. Shepherd, *Nat. Rev. Mater.* **2018**, *3*, 84.
[36] Z. He, C. Ren, A. Zhang, J. Bao, *J. Appl. Polym. Sci.* **2021**, *138*, 50908.
[37] T. J. Wallin, L.-E. Simonsen, W. Pan, K. Wang, E. Giannelis, R. F. Shepherd, Y. Mengüç, *Nat. Commun.* **2020**, *11*, 4000.
[38] K. Du, J. Basuki, V. Glattauer, C. Mesnard, A. T. Nguyen, D. L. J. Alexander, T. C. Hughes, *ACS Appl. Polym. Mater.* **2021**, *3*, 3049.
[39] J. Mewis, N. J. Wagner, *Adv. Colloid Interface Sci.* **2009**, *147–148*, 214.
[40] V. Ozbolat, M. Dey, B. Ayan, A. Povilianskas, M. C. Demirel, I. T. Ozbolat, *ACS Biomater. Sci. Eng.* **2018**, *4*, 682.
[41] H. Montazerian, M. Mohamed, M. M. Montazeri, S. Kheiri, A. Milani, K. Kim, M. Hoorfar, *Acta Biomater.* **2019**, *96*, 149.
[42] T. J. Hinton, A. Hudson, K. Pusch, A. Lee, A. W. Feinberg, *ACS Biomater. Sci. Eng.* **2016**, *2*, 1781.
[43] A. Nag, S. Feng, S. Mukhopadhyay, J. Kosel, D. Inglis, *Sens. Actuators, A* **2018**, *280*, 525.
[44] M. Moreno, J. Gonzalez-Rico, M. Lopez-Donaire, A. Arias, D. Garcia-Gonzalez, *Composites, Part B* **2021**, *224*, 109148.
[45] H. Wang, Z. Ouyang, L. Hu, Y. Cheng, J. Zhu, L. Ma, Y. Zhang, *Food Chem.* **2022**, *397*, 133725.
[46] L.-y. Zhou, Q. Gao, J.-z. Fu, Q.-y. Chen, J.-p. Zhu, Y. Sun, Y. He, *ACS Appl. Mater. Interfaces* **2019**, *11*, 23573.
[47] C. Zhao, Z. Xia, X. Wang, J. Nie, P. Huang, S. Zhao, *Mater. Des.* **2020**, *193*, 108788.
[48] N. R. Khatri, M. N. Islam, P.-F. Cao, R. C. Advincula, W. Choi, Y. Jiang, *Addit. Manuf.* **2021**, *48*, 102419.
[49] M. A. Skylar-Scott, J. Mueller, C. W. Visser, J. A. Lewis, *Nature* **2019**, *575*, 330.
[50] H. Yuk, B. Lu, S. Lin, K. Qu, J. Xu, J. Luo, X. Zhao, *Nat. Commun.* **2020**, *11*, 1604.
[51] C. Sturgess, C. J. Tuck, I. A. Ashcroft, R. D. Wildman, *J. Mater. Chem. C* **2017**, *5*, 9733.
[52] Q. Qian, J. H. Kamps, B. Price, H. Gu, R. Wildman, R. Hague, B. Begines, C. Tuck, *Addit. Manuf.* **2022**, *54*, 102745.
[53] A. K. Bastola, M. Hossain, *Composites, Part B* **2020**, *200*, 108348.
[54] T. Gao, G. J. Gillispie, J. S. Copus, A. Kumar Pr, Y.-J. Seol, A. Atala, J. J. Yoo, S. J. Lee, *Biofabrication* **2018**, *10*, 034106.
[55] A. Schwab, R. Levato, M. D'Este, S. Piluso, D. Eglin, J. Malda, *Chem. Rev.* **2020**, *120*, 11028.
[56] S. Lucarini, M. Moreno-Mateos, K. Danas, D. Garcia-Gonzalez, *Int. J. Solids Struct.* **2022**, *256*, 111981.
[57] F. N. Cogswell, *Polym. Eng. Sci.* **1972**, *12*, 64.